

DOI: 10.1002/cctc.201400096

Synthesis of Different Ruthenium Nickel Bimetallic Nanostructures and an Investigation of the Structure–Activity Relationship for Benzene Hydrogenation to Cyclohexane

Lihua Zhu,^[a] Maohong Cao,^[a] Li Li,^[a] Hanlei Sun,^[a] Yanqing Tang,^[a] Nuowei Zhang,^[a] Jinbao Zheng,^{*[a]} Hua Zhou,^[a] Yunhua Li,^[a] Lefu Yang,^[a] Chuan-Jian Zhong,^[b] and Bing H. Chen^{*[a]}

The catalytic properties of catalysts are generally highly dependent on their nanostructures in most heterogeneous catalytic reactions. Therefore, to acquire targeted catalytic activity, selectivity, and stability, catalysts with a specific nanostructure should be designed and synthesized. Herein, Ru-Ni bimetallic nanoparticles with different nanostructures, Ru-Ni alloy, Ru@Ni, and Ru clusters-on-Ni on carbon, have been synthesized by annealing Ru-Ni/C in flowing N₂+10% H₂ at different temperatures. The various nanostructures of the Ru-Ni bimetallic nano-

particles have been characterized and their catalytic behaviors were evaluated using benzene hydrogenation to cyclohexane. The relationship between the Ru-Ni bimetallic nanostructures and their catalytic performance is presented. It was found that Ru-Ni alloy/C and Ru clusters-on-Ni/C are much more active than Ru@Ni/C. This study also provides a simple method to design and control the nanostructures of the Ru-Ni bimetallic nanoparticles.

Introduction

Both in the past and at present, bimetallic catalysts are widely investigated in fundamental research^[1] and used in industrial catalysis processes.^[2] It is well known that the bimetallic nanostructure is one of the key factors to determine the catalytic behavior.^[3] Therefore, with the purpose to increase catalytic activity, selectivity, and durability, bimetallic catalysts with different expected nanostructures such as alloys, core–shell materials, and particles-on-particles have been prepared and utilized in numerous studies. For instance, Enache^[3e] synthesized Au-Pd(alloy)/TiO₂ nanocatalysts to achieve an unprecedented catalytic activity (turnover frequency (TOF) up to 270 000 h⁻¹) for the oxidation of alcohols to aldehydes compared to pure Au/TiO₂ or Pd/TiO₂ catalysts. Other alloy nanocatalysts, such as Pt-Co,^[4] Pt-Ni,^[5] Rh-Ni,^[6] Au-Pt,^[7] and Pt-Fe,^[8] have been exploited

in a series of reactions and exhibited distinguishing catalytic properties. Khashab et al. prepared hollow Au@Pd core–shell and hollow Au@Pt core–shell nanoparticles (NPs) by a galvanic displacement method.^[9] These two types of core–shell NPs showed a higher catalytic activity than those of monometallic Pt for the ethanol oxidation reaction in an alkaline medium. Au clusters were loaded onto carbon-supported Pt NPs by a galvanic replacement method by Adzic et al. The as-synthesized Au nanoparticles-on-Pt nanoparticles/C catalyst showed an unexpected stability (loss of 4% in electrochemical surface area after 30 000 cycles in a durability test) compared to a Pt/C catalyst for the oxygen reduction reaction.^[10] According to the above and plenty of other reported studies, it was found, and is perhaps becoming a generic view, that bimetallic nanocatalysts with a particular nanostructure provided a much better catalytic performance compared to the corresponding monometallic nanocatalysts.

Likewise, Ru-Ni bimetallic nanoparticles (BNPs) with different structures have been obtained in a few previous studies. We will take the following two reports as examples. The Ru-Ni core–shell was synthesized by a seeded growth method and it was applied in the ammonia borane hydrolysis reaction.^[11] Ru-Ni alloy NPs were obtained by adopting a colloidal synthetic approach and acted as a good catalyst for the dehydrogenation of ammonia borane.^[12] However, to the best of our knowledge, the synthesis of Ru-Ni alloy, Ru@Ni core–shell, and Ru clusters-on-Ni particles through the adjustment of the thermal treatment temperature on same precursor has not been reported to date.

[a] L. Zhu, M. Cao, L. Li, H. Sun, Y. Tang, Dr. N. Zhang, Dr. J. Zheng, Dr. H. Zhou, Dr. Y. Li, Dr. L. Yang, Prof. B. H. Chen
Department of Chemical and Biochemical Engineering
National Engineering Laboratory for Green
Productions of Alcohols-Ethers-Esters
College of Chemistry and Chemical Engineering
Xiamen University
Xiamen, 361005 (China)
Fax: (+86) 592-2184822
E-mail: jbzhang@xmu.edu.cn
chenbh@xmu.edu.cn

[b] Prof. C.-J. Zhong
Department of Chemistry
State University of New York at Binghamton
Binghamton, New York, 13902 (United States)

 Supporting information for this article is available on the WWW under <http://dx.doi.org/10.1002/cctc.201400096>.

In this study, carbon-supported Ni/Ni(OH)₂ NPs were obtained at room temperature (RT) by a hydrazine hydrate reduction method, and then Ru was deposited on Ni/Ni(OH)₂/C by a galvanic replacement reaction to form Ru-Ni/Ni(OH)₂/C. Additionally, various Ru-Ni nanostructures including Ru-Ni alloy, Ru@Ni, and Ru clusters-on-Ni particles were obtained successfully by simple variation of the annealing temperature in flowing N₂+10% H₂. The catalytic activity of the catalysts with different nanostructures has been evaluated by the reaction of benzene hydrogenation to cyclohexane. A structure–activity relationship has been established in this work for the benzene hydrogenation reaction system.

Results and Discussion

Preparation of the catalysts

The Ni/Ni(OH)₂/C sample was obtained at RT by the hydrazine hydrate reduction of nickel(II) chloride hexahydrate (NiCl₂·6H₂O) and using carbon black (BLACK PEARLS 2000 LOT-1366221) with a very high surface area (approximately 1385.3 m²g⁻¹) as the support with a Ni element loading of 16.84 wt%. The 16.84%Ni/C(380) was obtained after the Ni/Ni(OH)₂/C sample was annealed in N₂+10% H₂ at 380 °C for 3 h. The Ru-Ni/Ni(OH)₂/C sample was obtained by a galvanic replacement reaction with 1.25 wt% Ru loading, 15.75 wt% total Ni (Ni element) loading, and a Ru/Ni atomic ratio of 0.04/0.96. Ru-Ni/Ni(OH)₂/C was reduced in N₂+10% H₂ at different annealing temperatures (230, 280, 380, 480, 580, or 680 °C) for 3 h, denoted as Ru_{0.04}Ni_{0.96}/C(*T*). The 2.5%Ru/C(600) and 1.25%Ru/C(380) catalysts were prepared by incipient wetness impregnation for comparison. The synthesis steps are described in detail in the Experimental Section.

Catalyst characterization

The powder XRD patterns of 16.84%Ni/C(380), Ru_{0.04}Ni_{0.96}/C(*T*), and 2.5%Ru/C(600) are shown in Figure 1. Typical diffraction

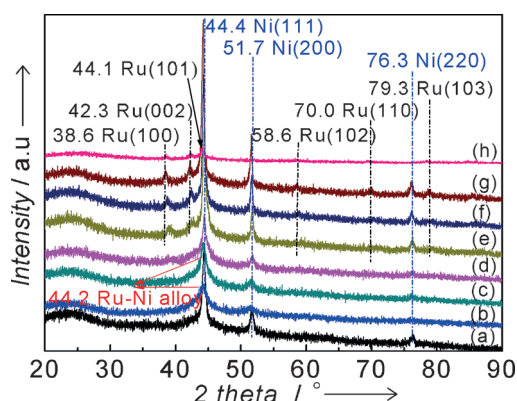


Figure 1. Powder XRD patterns of the Ru_{0.04}Ni_{0.96}/C(*T*) samples. a) 16.84%Ni/C(380), b) Ru_{0.04}Ni_{0.96}/C(230), c) Ru_{0.04}Ni_{0.96}/C(280), d) Ru_{0.04}Ni_{0.96}/C(380), e) Ru_{0.04}Ni_{0.96}/C(480), f) Ru_{0.04}Ni_{0.96}/C(580), g) Ru_{0.04}Ni_{0.96}/C(680), and h) 2.5%Ru/C(600). The blue and black dash-dot lines represent the diffraction peaks of the Ni and Ru crystallite phases, respectively.

peaks of the Ni(111) ($2\theta=44.4^\circ$), Ni(200) ($2\theta=51.7^\circ$), and Ni(220) ($2\theta=76.3^\circ$) planes (JCPDS card No. 04-0850) can be observed in Figure 1a, which indicates face-centered cubic (fcc) Ni in the 16.84%Ni/C(380) sample. For Ru_{0.04}Ni_{0.96}/C(230) and Ru_{0.04}Ni_{0.96}/C(280), only three diffraction peaks at $2\theta=44.2$, 51.6 , and 76.2° can be seen in Figure 1b and c, located between the corresponding Ni diffraction peaks in 16.84%Ni/C(380) (Figure 1a) and Ru diffraction peaks in 2.5%Ru/C(600) (Figure 1h). This indicates that Ru atoms have dissolved in fcc Ni to produce a Ru-Ni alloy, which results in the expansion of the lattice constant. With the increase of the annealing temperature to 380 °C, a weak diffraction peak of Ru(100) appears (JCPDS card No. 06-0663; Figure 1d), which suggests that some of the Ru atoms begin to segregate from the Ru-Ni alloy NPs. As the annealing temperature increases to 480 °C, the characteristic diffraction peaks of Ru(100) ($2\theta=38.6^\circ$) and Ru(002) ($2\theta=42.3^\circ$; JCPDS card No. 06-0663) become clear because of the complete phase segregation between Ru and Ni. Additionally, if the thermal treatment temperature increases continuously (e.g., to 580 and 680 °C), the XRD peaks of the pure Ni and Ru crystallite phases are shifted to lower angles, which indicates clearly that high temperatures improve the lattice constant expansion.^[13] Moreover, the intensity of the peaks increases gradually, and the full-width at half-maximum is increased with the increase of temperature, which suggests that the degree of crystallinity and the size of the Ru-Ni BNPs increase. Magnifications of the XRD patterns in the regions 40–50, 45–65, and 65–85° are presented in Figure S1, in which the shifts of the characteristic diffraction peaks are clearer.

The lattice parameters of different catalysts are calculated from the Ni(111) diffraction peak position. The relationship between the annealing temperature and lattice parameter is displayed in Figure 2. Based on this plot, it can be found that the lattice parameter of Ni for the Ru_{0.04}Ni_{0.96}/C(*T*) catalysts is larger than that for 16.84%Ni/C(380) if the treatment temperature is in the range of 230–380 °C. This is because some Ru atoms dissolve in fcc Ni to result in the lattice expansion. At 480 °C, the lattice parameter decreases to less than that of the 16.84%Ni/C(380) catalyst, which indicates the complete phase segregation of Ru and Ni. If the thermal treatment temperature increases above 480 °C (e.g., 580 or 680 °C), the increase of the

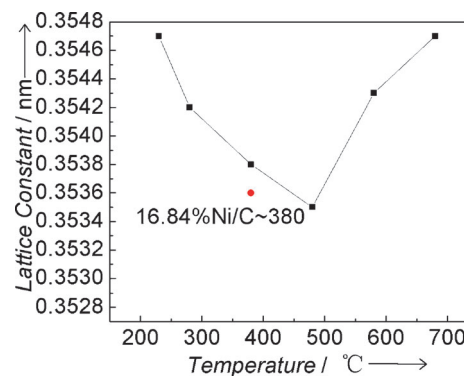


Figure 2. Relationship between the annealing temperature and lattice parameters of the catalysts.

lattice parameter is a result of the high temperature, which encourages the lattice expansion.^[13]

Therefore, the evolution of the Ru-Ni nanostructure with the thermal treatment temperature can be demonstrated clearly by the above XRD results. If the annealing temperature of the Ru_{0.04}Ni_{0.96}/C(T) catalysts is 230 or 280 °C, complete Ru-Ni alloy NPs were formed. Partial Ru-Ni alloy and partial Ru-Ni phase segregation are obtained at 380 °C. Finally, at 480, 580, and 680 °C, complete Ru-Ni phase segregation is achieved. The accurate nanostructures of the Ru-Ni BNPs have also been characterized by other techniques.

X-ray photoelectron spectroscopy (XPS) measurements were performed to obtain the chemical states of Ru and Ni in the different catalysts. As displayed in the Ni2p XPS spectrum (Figure 3A), it is well known that the binding energies at 861.8 and 880.5 eV are ascribed to multi-electron excitation.^[14] For these three samples, 16.84%Ni/C(380), Ru_{0.04}Ni_{0.96}/C(480), and Ru_{0.04}Ni_{0.96}/C(680), the binding energies of 852.7, 853.9, 855.4, and 857.1 eV in the Ni2p_{3/2} XPS spectrum are caused by Ni⁰, NiO, Ni(OH)₂, and NiOOH species, respectively. The other peaks at binding energies of 870, 871.2, 872.9, and 874.4 eV in the Ni2p_{1/2} XPS spectrum are ascribed to Ni⁰, NiO, Ni(OH)₂, and NiOOH species, respectively.^[14–15] On comparing the intensity of each peak, the main Ni species in all the samples are found to be of varying oxidation state as Ni–NiO, Ni(OH)₂, and NiOOH. The NiO originates mainly from the oxidation of Ni NPs in air,^[15d] and the formation of Ni(OH)₂ was probably because of the reaction of NiO with H₂O in air. NiOOH was formed as Ni(OH)₂ was further oxidized in air. However, for the Ru_{0.04}Ni_{0.96}/C(230) sample, the binding energy at 852.5 eV corresponds to Ni⁰ with a 0.2 eV shift to a lower binding energy relative to the 16.84%Ni/C(380) or Ru_{0.04}Ni_{0.96}/C(680) samples because of the

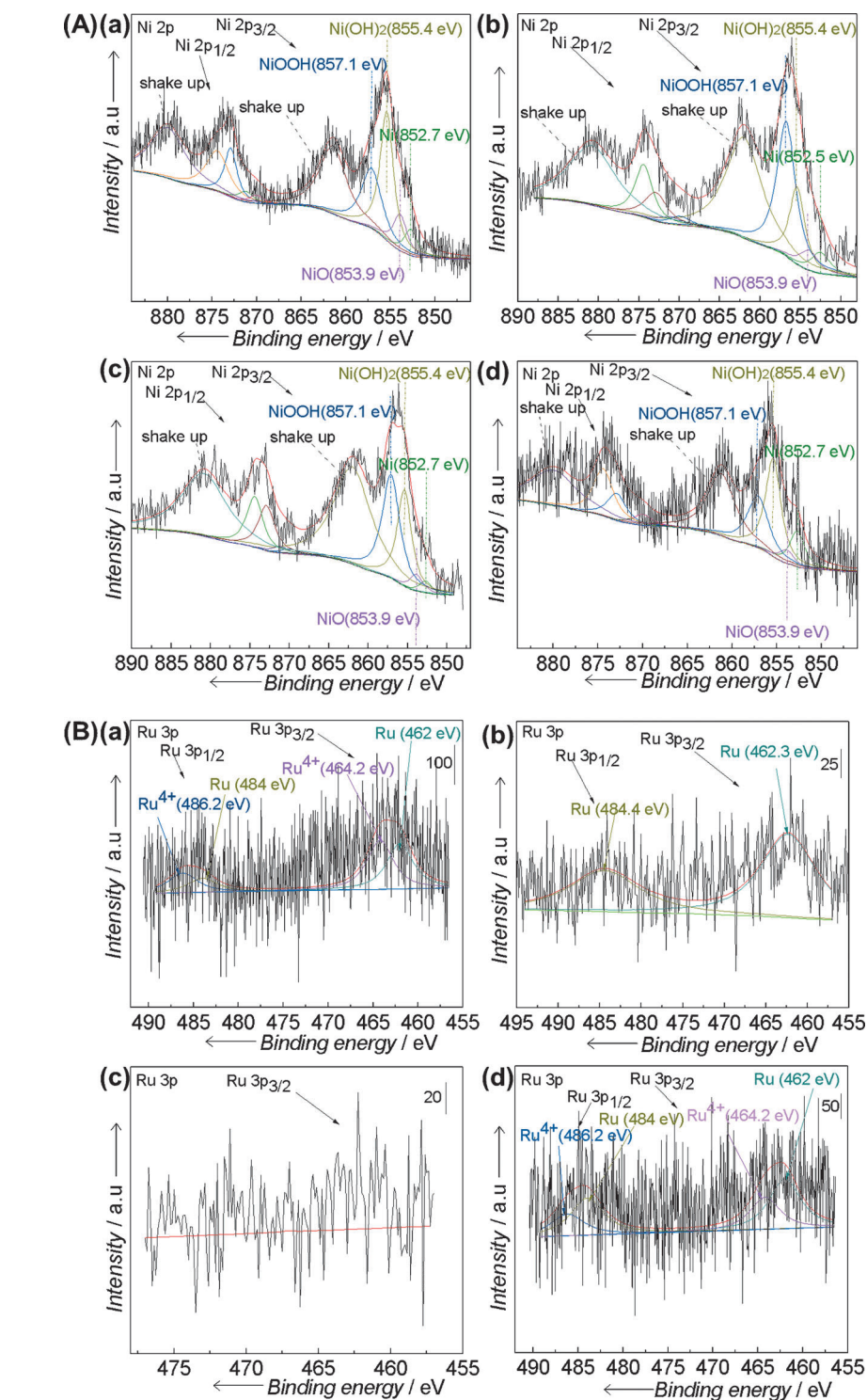


Figure 3. XPS spectra. A), a) Ni2p edge in 16.84%Ni/C(380), b) Ni2p edge in Ru_{0.04}Ni_{0.96}/C(230), c) Ni2p edge in Ru_{0.04}Ni_{0.96}/C(480), d) Ni2p edge in Ru_{0.04}Ni_{0.96}/C(680). B), a) Ru3p edge in 1.25%Ru/C(380), b) Ru3p edge in Ru_{0.04}Ni_{0.96}/C(230), c) Ru3p edge in Ru_{0.04}Ni_{0.96}/C(480), d) Ru3p edge in Ru_{0.04}Ni_{0.96}/C(680).

transfer of an electron from Ru to Ni.^[16] This suggests that Ru-Ni alloy NPs are produced in this catalyst. Although all the catalysts were reduced in N₂+10% H₂, a lot of oxidized Ni was still detected on the catalyst surface by XPS after exposure to air, which indicates the existence of many Ni atoms on the surface of these catalysts. XPS binding energies and the relative

composition [mol%] of different Ni species (Ni^0 , NiO , Ni(OH)_2 , and NiOOH) on the surface of the catalysts are shown in Table S1.

Generally, it is well known that the Ru3d spectrum is not clear as it is often obscured by the strong C 1s signal.^[17] Therefore, the XPS test for Ru was conducted between 458 and 472 eV in which Ru3p peaks are expected to be observed (Figure 3B). For the 1.25%Ru/C(380) and $\text{Ru}_{0.04}\text{Ni}_{0.96}/\text{C}$ (680) catalysts, the peak positions at binding energies of 462 and 464.2 eV in the Ru3p_{3/2} XPS spectra are assigned to Ru^0 and RuO_2 . The other two peaks at higher energies (484 and 486.2 eV) in the Ru3p_{1/2} XPS spectra are also contributed to by Ru^0 and oxidized RuO_2 , respectively.^[18] The presence of RuO_2 was a result of the surface oxidation of Ru^0 NP after exposure to air prior to characterization,^[19] which demonstrates that there are Ru atoms on the surface of the Ru-Ni BNPs in $\text{Ru}_{0.04}\text{Ni}_{0.96}/\text{C}$ (680). However, for the $\text{Ru}_{0.04}\text{Ni}_{0.96}/\text{C}$ (230) sample, the binding energy of Ru^0 in the Ru3p_{3/2} XPS spectrum is shifted to a higher energy position (462.3 eV) compared to that of 1.25%Ru/C(380), which is almost without a RuO_2 signal. This suggests that the Ru-Ni alloy NPs are formed in the $\text{Ru}_{0.04}\text{Ni}_{0.96}/\text{C}$ (230) sample, which prevents the oxidation of Ru in air. However, the XPS signal of the Ru species was very weak in the $\text{Ru}_{0.04}\text{Ni}_{0.96}/\text{C}$ (480) sample, which confirms that Ru was probably present as a core inside the Ni particles (Ru@Ni) and was difficult to detect by the XPS method. XPS binding energies and relative compositions [mol%] of the different Ru species (Ru^0 and RuO_2) on the surface of the catalysts are shown in Table S2.

TEM images of $\text{Ru}_{0.04}\text{Ni}_{0.96}/\text{C}$ (230), $\text{Ru}_{0.04}\text{Ni}_{0.96}/\text{C}$ (480), and $\text{Ru}_{0.04}\text{Ni}_{0.96}/\text{C}$ (680) are shown in Figure S2. The mean size of the Ru-Ni BNPs in the $\text{Ru}_{0.04}\text{Ni}_{0.96}/\text{C}$ (230) sample was controlled at 11.56 nm with a relatively narrow size distribution (Figure S2A and B), whereas, if $\text{Ru}_{0.04}\text{Ni}_{0.96}/\text{C}$ (T) was reduced in $\text{N}_2+10\% \text{H}_2$ at 480 °C for 3 h, the average size of the Ru-Ni BNPs increased to 14.06 nm also with a relatively narrow size distribution (Figure S2C and D). However, for the $\text{Ru}_{0.04}\text{Ni}_{0.96}/\text{C}$ (680) catalyst, the mean size of the Ru-Ni BNPs is the same as that of the $\text{Ru}_{0.04}\text{Ni}_{0.96}/\text{C}$ (480) sample but with a wider size distribution (Figure S2E and F). To explore the relationship between the annealing temperature and the Ru-Ni bimetallic nanostructure, high-resolution transmission electron microscopy (HRTEM) images were obtained of these three samples. The HRTEM images of $\text{Ru}_{0.04}\text{Ni}_{0.96}/\text{C}$ (230) reveal lattice fringes with a regular spacing of 0.209 nm (Figure 4A and B). This spacing is located between the lattice fringe distances of Ru(100) (0.234 nm) or Ru(002) (0.214 nm; JCPDS card No. 06-0663) and that of Ni(111) (0.203 nm; JCPDS card No. 04-0850), which indicates the formation of a Ru-Ni alloy. However, with the increase of the annealing temperature to 480 °C, the HRTEM image of an individual Ru-Ni BNP shows lattice fringes with an interplanar spacing of 0.170 nm (Figure 4C and D) ascribed to Ni(200) fringes of fcc Ni (JCPDS card No. 04-0850). In the HRTEM image of the $\text{Ru}_{0.04}\text{Ni}_{0.96}/\text{C}$ (680) sample, the lattice fringe distance of 0.203 nm is observed clearly (Figure 4E and F), which is a result of Ni(111) facets (JCPDS card No. 04-0850). These HRTEM images of the $\text{Ru}_{0.04}\text{Ni}_{0.96}/\text{C}$ (480) and $\text{Ru}_{0.04}\text{Ni}_{0.96}/\text{C}$ (680)

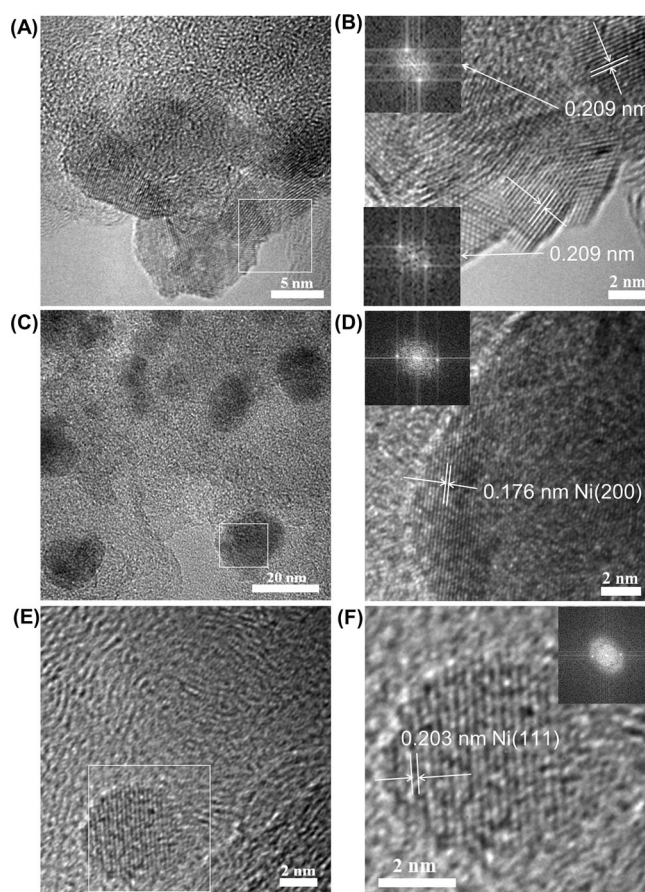
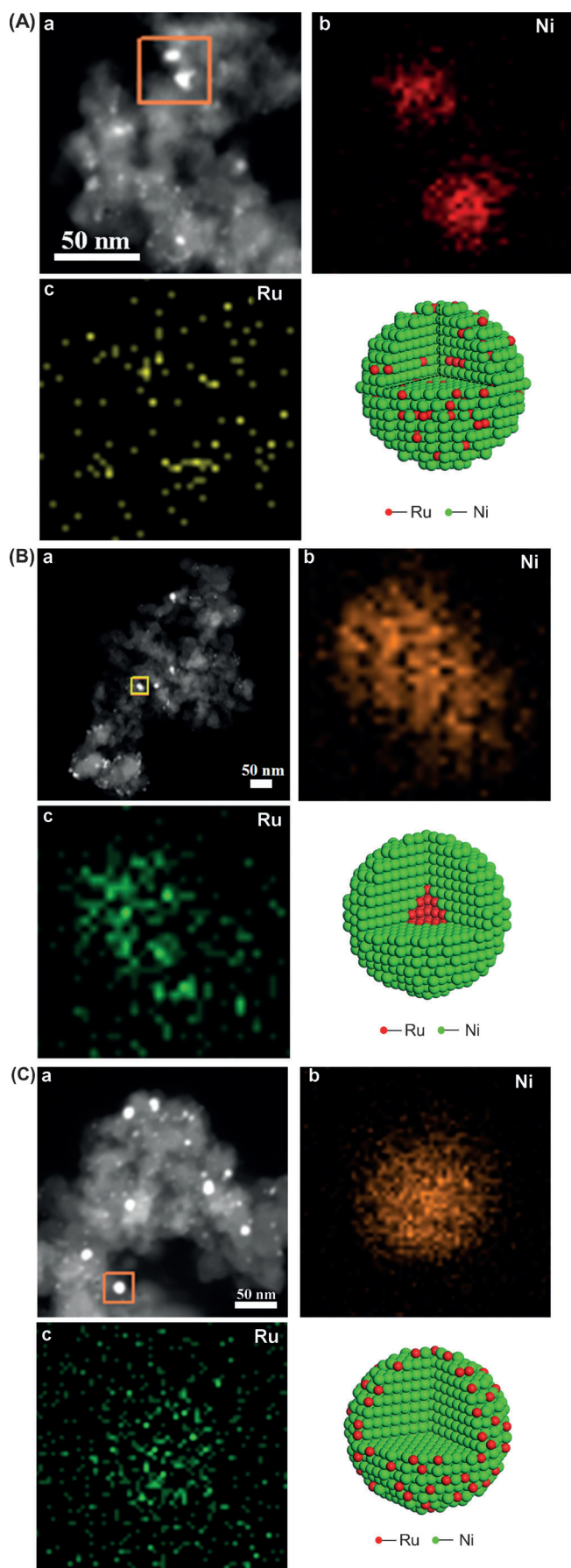


Figure 4. HRTEM images of the $\text{Ru}_{0.04}\text{Ni}_{0.96}/\text{C}$ (T) catalysts. A) HRTEM image of $\text{Ru}_{0.04}\text{Ni}_{0.96}/\text{C}$ (230). B) Enlarged view of the selected area in A. The indicated lattice fringes, 0.209 nm (between 0.203 nm Ni(111) (JCPDS card No. 04-0850) and 0.214 nm Ru(002) or 0.234 nm Ru(100) (JCPDS card No. 06-0663), which correspond to Ru-Ni alloy. C) HRTEM image of $\text{Ru}_{0.04}\text{Ni}_{0.96}/\text{C}$ (480). D) Enlarged view of the selected area in C. The indicated lattice fringe, 0.176 nm, is ascribed to Ni(200) planes (JCPDS card No. 04-0850). E) HRTEM image of $\text{Ru}_{0.04}\text{Ni}_{0.96}/\text{C}$ (680). F) Enlarged view of the selected area in E. The indicated lattice fringe, 0.203 nm, is attributed to Ni(111) facets (JCPDS card No. 04-0850). The insets show the respective fast Fourier transform (FFT) patterns.

catalysts further illustrate the Ru-Ni phase segregation in these two samples.

As it is difficult to distinguish Ni from Ru in HRTEM images (Figure 4) because of the indistinct contrast between these two elements, elemental analysis was performed by high-angle annular dark-field scanning transmission electron microscopy (HAADF-STEM) combined with energy-dispersive X-ray spectroscopy (EDS) to further establish the Ru-Ni nanostructures and elemental distributions in the $\text{Ru}_{0.04}\text{Ni}_{0.96}/\text{C}$ (230), $\text{Ru}_{0.04}\text{Ni}_{0.96}/\text{C}$ (480), and $\text{Ru}_{0.04}\text{Ni}_{0.96}/\text{C}$ (680) catalysts. A representative HAADF-STEM image and its corresponding Ru and Ni elemental maps of $\text{Ru}_{0.04}\text{Ni}_{0.96}/\text{C}$ (230) are presented in Figure 5A, which demonstrate that the distribution ranges of Ni and Ru could overlap to some extent. Based on the XRD and XPS results for the $\text{Ru}_{0.04}\text{Ni}_{0.96}/\text{C}$ (230) sample, a conclusion can be drawn that the as-synthesized $\text{Ru}_{0.04}\text{Ni}_{0.96}/\text{C}$ (230) is definitely Ru-Ni alloy/C. An HAADF-STEM image and elemental maps of Ru and Ni for the $\text{Ru}_{0.04}\text{Ni}_{0.96}/\text{C}$ (480) catalyst are shown in Fig-



ure 5B, and it can be observed clearly that Ru (green) is surrounded by Ni (orange). This probably indicates that a Ru@Ni core-shell structure was formed in this sample. The HAADF-STEM image and elemental analysis for Ru_{0.04}Ni_{0.96}/C(680) is displayed in Figure 5C, which suggest that the distribution of Ru and Ni are homogenous. However, the foregoing XRD results for Ru_{0.04}Ni_{0.96}/C(680) (Figure 1 h) did not reveal the presence of a Ru-Ni alloy. This indicates that Ru atoms are supported on the Ni NPs in this sample. Structural models of these three catalysts are also presented in Figure 5, which demonstrate vividly the different nanostructures in these samples. These conclusions were further verified by a high-sensitivity low-energy ion scattering (HS-LEIS) study.

To obtain further information on the different structures of our as-prepared Ru_{0.04}Ni_{0.96}/C(7) catalysts, HS-LEIS measurements were performed because this technique can effectively provide the atomic composition of the outmost atomic layer of the solid surface.^[20] The 5 keV ²⁰Ne⁺ HS-LEIS spectra of Ru_{0.04}Ni_{0.96}/C(230), Ru_{0.04}Ni_{0.96}/C(480), and Ru_{0.04}Ni_{0.96}/C(680) are presented in Figure 6. Ru and Ni atoms coexist on the outmost surface of the Ru_{0.04}Ni_{0.96}/C(230) catalyst, but the quantity of Ni atoms is much larger than that of the Ru atoms (Figure 6a), whereas only the Ni signal appeared on the outer surface of the Ru_{0.04}Ni_{0.96}/C(480) sample (Figure 6b). As the Ru_{0.04}Ni_{0.96}/C (uncalcined) catalyst was reduced at a higher temperature (e.g., 680 °C), the Ru and Ni signals can be observed at the same time in the HS-LEIS spectra for the Ru_{0.04}Ni_{0.96}/C(680) catalyst (Figure 6c). Therefore, these HS-LEIS results provide further evidence that the evolution of the Ru-Ni bimetallic nanostructure is highly dependent on the thermal treatment temperature.

Based on the above characterizations, it can be concluded that Ru-Ni alloy is formed in the Ru_{0.04}Ni_{0.96}/C(230) sample, Ru@Ni core-shell particles is generated in the Ru_{0.04}Ni_{0.96}/C(480) sample, and Ru clusters-on-Ni particles are obtained in the Ru_{0.04}Ni_{0.96}/C(680) sample.

A schematic illustration of the evolution of the Ru-Ni bimetallic nanostructure of the Ru_{0.04}Ni_{0.96}/C(7) catalysts is depicted in Scheme 1. The evolution process is described as follows. Firstly, Ni(OH)₂ is produced by the combination of Ni²⁺ ions with OH⁻ ions; secondly, a small number of Ni²⁺ ions were formed gradually from the dissociation of Ni(OH)₂ with a low dissociation constant and were reduced to Ni⁰ at RT by hydrazine hydrate, and the Ni/Ni(OH)₂ was supported on the carbon black. Thirdly, some of the Ni atoms would be displaced with Ru atoms by a replacement reaction after the addition of aque-

Figure 5. A) HAADF-STEM image and elemental mapping for several Ru-Ni BNPs in Ru_{0.04}Ni_{0.96}/C(230). a) HAADF-STEM image of Ru_{0.04}Ni_{0.96}/C(230), b) and c) EDS maps of Ni (red) and Ru (yellow), respectively, d) structural model of Ru_{0.04}Ni_{0.96}/C(230); B) HAADF-STEM image and elemental mapping for an individual Ru-Ni BNP in Ru_{0.04}Ni_{0.96}/C(480). a) HAADF-STEM image of Ru_{0.04}Ni_{0.96}/C(480), b) and c) EDS maps of Ni (orange) and Ru (green), respectively, d) structural model of Ru_{0.04}Ni_{0.96}/C(480); C) HAADF-STEM image and elemental mapping for an individual Ru-Ni BNP in Ru_{0.04}Ni_{0.96}/C(680). a) HAADF-STEM image of an individual Ru-Ni BNP, b) and c) EDS maps of Ni (orange) and Ru (green), respectively, d) structural model of Ru_{0.04}Ni_{0.96}/C(680).

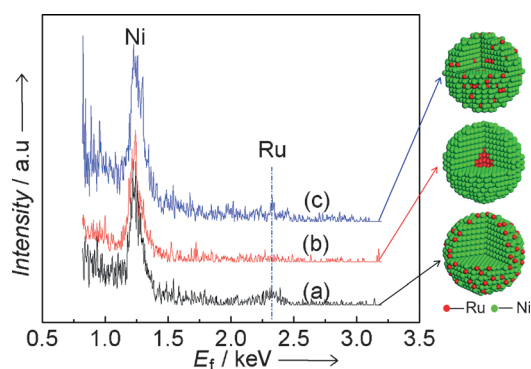
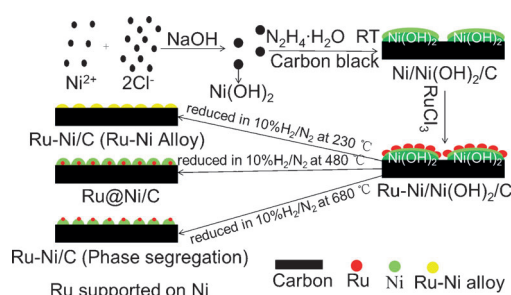


Figure 6. HS-LEIS spectra (5 keV $^{20}\text{Ne}^+$) of a) $\text{Ru}_{0.04}\text{Ni}_{0.96}/\text{C}(230)$, b) $\text{Ru}_{0.04}\text{Ni}_{0.96}/\text{C}(480)$, and c) $\text{Ru}_{0.04}\text{Ni}_{0.96}/\text{C}(680)$. E_f = Energy of backscattered ion.



Scheme 1. Schematic illustration of the evolution of Ru-Ni alloy, Ru@Ni, and Ru clusters-on-Ni particles supported on carbon black.

ous RuCl_3 solution to form $\text{Ru-Ni}/\text{Ni}(\text{OH})_2/\text{C}$. Finally, the $\text{Ru}_{0.04}\text{Ni}_{0.96}/\text{C}(T)$ catalysts with different nanostructures were obtained after they were annealed in flowing $\text{N}_2+10\% \text{H}_2$ (80 mL min^{-1}) at various temperatures for 3 h.

Catalytic performance of $\text{Ru}_{0.04}\text{Ni}_{0.96}/\text{C}(T)$ for benzene hydrogenation

The catalytic performance of various catalysts for the reaction of benzene hydrogenation to cyclohexane was measured under relatively mild conditions (reaction pressure, 5.3 MPa H_2 ; reaction temperature, 60°C ; reaction time, 1 h). All of the as-prepared catalysts gave 100% selectivity to cyclohexane (Table 1). For the 16.84%Ni/C(380) sample, no product was produced (Table 1, entry 1). However, the $\text{Ru}_{0.04}\text{Ni}_{0.96}/\text{C}(230)$ catalyst provided a 9.25% yield to cyclohexane with a relatively high TOF of 1684.5 h^{-1} (Table 1, entry 2), which was approximately 17 times more activity than that of the $\text{Ru}_{0.04}\text{Ni}_{0.96}/\text{C}(480)$ sample (Table 1, entry 3). This reaction was also conducted over the $\text{Ru}_{0.04}\text{Ni}_{0.96}/\text{C}(680)$ catalyst under the same reaction conditions, which showed a lower activity (Table 1, entry 4; 6.77% yield to cyclohexane and a TOF of 1232.8 h^{-1}) compared to $\text{Ru}_{0.04}\text{Ni}_{0.96}/\text{C}(230)$. Moreover, $\text{Ru}_{0.04}/\text{C}(680)$ gave a 3.35% yield to cyclohexane and a TOF of 610.6 h^{-1} (Table 1, entry 5) in the benzene hydrogenation reaction. The catalytic activity of the catalysts was in the order: $\text{Ru}_{0.04}\text{Ni}_{0.96}/$

$\text{C}(230)$ (Ru-Ni alloy) $\approx \text{Ru}_{0.04}\text{Ni}_{0.96}/\text{C}(680)$ (Ru clusters-on- Ni particles) $> \text{Ru}_{0.04}/\text{C}(680) > \text{Ru}_{0.04}\text{Ni}_{0.96}/\text{C}(480)$ (Ru@Ni). Clearly, the catalytic performance is highly dependent on the Ru-Ni bimetallic nanostructure. Such dependence could be explained by the following principles. It is generally accepted that a monometallic Ru catalyst is more active than a monometallic Ni catalyst for the activation and dissociation of hydrogen molecules under relatively mild reaction conditions. Furthermore, Ru-based catalysts are currently considered as highly effective catalysts for the benzene hydrogenation reaction.^[19,21] Hence, if Ru atoms are on the surface of the Ru-Ni BNPs in the $\text{Ru}_{0.04}\text{Ni}_{0.96}/\text{C}(230)$ (Ru-Ni alloy) and $\text{Ru}_{0.04}\text{Ni}_{0.96}/\text{C}(680)$ (Ru clusters-on- Ni particles) catalysts, it could facilitate the activation and dissociation of hydrogen molecules, which would improve their catalytic performance for benzene hydrogenation. However, the $\text{Ru}_{0.04}\text{Ni}_{0.96}/\text{C}(480)$ (Ru@Ni) catalyst exhibited no activity for this reaction because many of the Ru atoms were in the core of the Ru@Ni NPs. The catalytic properties of $\text{Ru}_{0.04}\text{Ni}_{0.96}/\text{C}(680)$ were a little poorer than those of $\text{Ru}_{0.04}\text{Ni}_{0.96}/\text{C}(230)$, which could be attributed to the larger size of the Ru-Ni BNPs (Figure S2).

Stability of the $\text{Ru}_{0.04}\text{Ni}_{0.96}/\text{C}(T)$ catalysts for benzene hydrogenation

The stability of the $\text{Ru}_{0.04}\text{Ni}_{0.96}/\text{C}(T)$ catalysts was also investigated in this work. The $\text{Ru}_{0.04}\text{Ni}_{0.96}/\text{C}(230)$, $\text{Ru}_{0.04}\text{Ni}_{0.96}/\text{C}(480)$, and $\text{Ru}_{0.04}\text{Ni}_{0.96}/\text{C}(680)$ catalysts were reused for another four runs under the same reaction conditions (reaction pressure, 5.3 MPa H_2 ; reaction temperature, 60°C ; reaction time, 1 h). No clear deactivation was seen from the results shown in Figure S3, especially if we take the possibility of tiny catalyst loss during reagents–catalyst separation into account. Additionally, the HRTEM images of the $\text{Ru}_{0.04}\text{Ni}_{0.96}/\text{C}(T)$ ($X=230, 480$, and 680) catalysts after five uses are displayed in Figure S4. These images confirm that the $\text{Ru}_{0.04}\text{Ni}_{0.96}/\text{C}(230)$ catalyst is still in the form of Ru-Ni alloy NPs, $\text{Ru}_{0.04}\text{Ni}_{0.96}/\text{C}(480)$ - Ru@Ni is still core-shell, and $\text{Ru}_{0.04}\text{Ni}_{0.96}/\text{C}(680)$ is still Ru clusters-on-Ni particles, which suggests that the nanostructures of the Ru-Ni BNPs are very stable during the reaction. The reasons for the excellent stability of the nanostructures of Ru-Ni BNPs are as follows:

Table 1. Catalytic performances of the $\text{Ru}_{0.04}\text{Ni}_{0.96}/\text{C}(T)$ catalysts under the same reaction conditions for benzene hydrogenation to cyclohexane.^[a]

Entry	Catalyst (0.05 g)	T [$^\circ\text{C}$]	TOF [h^{-1}]	Yield to cyclohexane [%]
1	16.84%Ni/C(380)	60	–	< 0.1
2	$\text{Ru}_{0.04}\text{Ni}_{0.96}/\text{C}(230)$	60	1684.5	9.25
3	$\text{Ru}_{0.04}\text{Ni}_{0.96}/\text{C}(480)$	60	96.5	0.53
4	$\text{Ru}_{0.04}\text{Ni}_{0.96}/\text{C}(680)$	60	1232.8	6.77
5	$\text{Ru}_{0.04}/\text{C}(680)$ ^[b]	60	610.6	3.35

[a] All reactions were conducted under the following conditions: benzene (10 mL), reaction time (1 h), reaction pressure (5.3 MPa). All of the as-prepared catalysts gave 100% selectivity to cyclohexane. [b] $\text{Ru}_{0.04}/\text{C}(680)$ was prepared by incipient wetness impregnation using carbon as the support and reduced in $\text{N}_2+10\% \text{H}_2$ at 680°C for 3 h.

1) these catalysts were annealed in $N_2+10\% H_2$ at high temperature (above $230^\circ C$) for 3 h, which is much higher than the reaction temperature ($60^\circ C$); 2) the annealing atmosphere of the catalysts is the same as the reaction atmosphere (H_2).

Conclusions

Ru-Ni bimetallic nanoparticles (BNPs) with different nanostructures, Ru-Ni alloy, Ru@Ni, and Ru clusters-on-Ni particles, supported on carbon were synthesized successfully by the simple method of changing the reducing temperature to 230, 480, and $680^\circ C$, correspondingly. The nanostructures of these catalysts were characterized by XRD, X-ray photoelectron spectroscopy, high-resolution transmission electron microscopy, energy-dispersive spectroscopy mapping, and high-sensitivity low-energy ion scattering measurements. The order of the catalytic performance for the hydrogenation of benzene to cyclohexane was $Ru_{0.04}Ni_{0.96}/C(230)$ (Ru-Ni alloy) $\approx Ru_{0.04}Ni_{0.96}/C(680)$ (Ru clusters-on-Ni particles) $> Ru_{0.04}Ni_{0.96}/C(480)$ (Ru@Ni). In addition, the nanostructures of the Ru-Ni BNPs are very stable in the reaction. The correlation between the nanostructure and the catalytic activity of the catalyst for the hydrogenation of benzene to cyclohexane was established in this work. The thermal treatment method to tune the Ru-Ni bimetallic nanostructure is likely to be extended to other BNPs, which is expected to have profound implications in other catalytic reaction systems.

Experimental Section

Materials

Carbon (BLACK PEARLS 2000 LOT-1366221) was obtained from Cabot Corporation. All other reagents ($NiCl_2 \cdot 6H_2O$, anhydrous ethanol, NaOH, anhydrous $RuCl_3$, polyvinyl pyrrolidone (PVP), and 85 wt% hydrazine hydrate solution) were supplied by Sinopharm Chemical Reagent Co. Ltd. (Shanghai, China). The water used in all experiments was deionized water produced by a Milli-Q Integral 3 (Millipore Corporation). CO (99.5%), H_2 (99.999%), and $N_2+10\% H_2$ were purchased from Linde Gas (Xiamen) Co. Ltd. All reagents were used as received.

Catalyst synthesis

Firstly, $Ni/Ni(OH)_2/C$ was prepared by a hydrazine reduction method, using carbon black as the support with a very high surface area (approximately $1385.3 m^2 g^{-1}$).^[22] $Ni/Ni(OH)_2/C$ was prepared by the following procedure. PVP (0.300 g) and anhydrous ethanol (12.5 mL) were mixed with a certain amount of aqueous $NiCl_2 \cdot 6H_2O$ solution with a concentration of $4.6 \times 10^{-2} mol L^{-1}$ with magnetic stirring at RT for 10 min. Then, aqueous NaOH solution (1.813 g of NaOH dissolved in 12.5 mL of deionized water) was added to the above green solution. After 10 min, 85 wt% hydrazine hydrate solution (25 mL) was added. Subsequently, carbon black (1.250 g) was suspended in the as-obtained liquid. The above liquid was transferred into a Teflon cup and agitated vigorously at RT for 18 h. The obtained solids were recovered by filtration and washed repeatedly with deionized water and anhydrous ethanol until no chlorine ions were detected. $Ni/Ni(OH)_2/C$ was obtained after drying in vacuum at $60^\circ C$ for 6 h. The Ni loading was

16.84 wt% (including Ni element in $Ni(OH)_2$) determined by inductively coupled plasma mass spectrometry (ICP-MS). The Ru-Ni/ $Ni(OH)_2/C$ catalysts were prepared by galvanic replacement reactions by adding a certain amount of aqueous $RuCl_3$ solution ($9.64 \times 10^{-3} mol L^{-1}$) into $Ni/Ni(OH)_2/C$ and Ru atoms were anchored onto $Ni/Ni(OH)_2$. The catalyst had a Ru/Ni atomic ratio of 4:96, a Ru loading of 1.25 wt%, and a Ni loading of 15.57 wt% (determined by ICP-MS). The Ru-Ni/ $Ni(OH)_2/C$ catalysts were then reduced in flowing $N_2+10\% H_2$ ($80 mL min^{-1}$) at various annealing temperatures for 3 h with a heating rate of $2^\circ C min^{-1}$. The products were denoted as $Ru_{0.04}Ni_{0.96}/C(T)$, in which $T_{annealing} = 230, 280, 380, 480, 580, \text{ or } 680^\circ C$. Ru/C catalysts with a Ru loading of 1.25 or 2.5 wt% were prepared by incipient wetness impregnation using carbon black as the support and then reduced in flowing $N_2+10\% H_2$ ($80 mL min^{-1}$) at 380 or $600^\circ C$ for 3 h, and the products denoted as 1.25%Ru/C(380) or 2.5%Ru/C(600), respectively.

Characterization

Powder XRD patterns for the samples were collected by using a Rigaku Ultima IV X-ray diffractometer equipped with a high-speed array detection system, and CuK_α radiation (35 kV and 20 mA) was used as the X-ray source. Scans were performed over the 2θ range of $20-90^\circ$ with a scanning rate of $20^\circ min^{-1}$. XPS measurements were performed by using a PHI Quantum 2000 Scanning ESCA Microprobe equipment with monochromatic AlK_α radiation (1846.6 eV) as the X-ray source. TEM and HRTEM studies of the catalysts were performed by using a TECNAI F30-HRTEM with a field-emission source, and the accelerating voltage was 300 kV. HAADF-STEM and STEM-EDS mapping analysis was also performed by using a TECNAI F20-HRTEM equipped with a field-emission source, and the accelerating voltage was 200 kV. HS-LEIS measurements were performed by using a $^{20}Ne^+$ beam energy of 5 keV, a sample current of 1.6 nA. The scattering angle was 145° .

Catalytic activity tests

The hydrogenation of benzene to cyclohexane was performed in a stainless-steel, high-pressure reactor (Parr 4848) with a magnetic stirrer. A mixture of benzene (10 mL) and catalyst (50 mg) was added into the reactor, which was then sealed immediately. H_2 (4.8 MPa) was introduced into the autoclave after it was purged with N_2 for 1 min and then with H_2 for 1 min. The stirring rate was approximately 500 rpm. The mixture was heated quickly to the required temperature ($60^\circ C$) and the H_2 pressure was increased to 5.3 MPa. After the desired reaction time (1 h), the reactor was cooled quickly to approximately $5^\circ C$ by using an ice-water bath, and then the autoclave was evacuated. The catalysts were separated from the liquid by centrifugation. The products were analyzed by GC by using a Shimadzu GC 2010 instrument equipped with a DB-35 60 m \times 0.32 mm capillary column and a flame ionization detector (FID), and GC-MS (Shimadzu GC-MS 2010) was used if necessary. The TOF of the catalysts was calculated from Equation (1):

$$TOF_{Ru-Ni} = \frac{n_{conversion}}{t \times n_{Ru}}; \quad TOF_{Ni} = \frac{n_{conversion}}{t \times n_{Ni}} \quad (1)$$

in which $n_{conversion}$ is the conversion of benzene [mol], t is the reaction time, n_{Ru} is the number of moles of Ru, and n_{Ni} is the number of moles of ruthenium and nickel. TOF_{Ni} and TOF_{Ru} represent the TOF of the 16.84%Ni/C(380) and $Ru_{0.04}Ni_{0.96}/C(680)$, $Ru_{0.04}/C(680)$ catalysts, respectively.

Acknowledgements

The authors would like to thank the National Natural Science Foundation of China (Grant 20973140, 201106118, and 21303140) for financial support.

Keywords: hydrogenation · nanoparticles · nickel · ruthenium · structure–activity relationships

- [1] a) B. Lim, M. Jiang, P. H. C. Camargo, E. C. Cho, J. Tao, X. Lu, Y. Zhu, Y. Xia, *Science* **2009**, *324*, 1302–1305; b) H. Zhang, T. Watanabe, M. Okumura, M. Haruta, N. Toshima, *Nat. Mater.* **2012**, *11*, 49–52; c) T. R. Johns, J. R. Gaudet, E. J. Peterson, J. T. Miller, E. A. Stach, C. H. Kim, M. P. Balogh, A. K. Datye, *ChemCatChem* **2013**, *5*, 2636–2645; d) L. Delannoy, S. Giorgio, J. G. Mattei, C. R. Henry, N. El Kolli, C. Méthivier, C. Louis, *ChemCatChem* **2013**, *5*, 2707–2716; e) L. Gan, S. Rudi, C. Cui, P. Strasser, *ChemCatChem* **2013**, *5*, 2691–2694.
- [2] a) D. M. Alonso, S. G. Wettstein, J. A. Dumesic, *Chem. Soc. Rev.* **2012**, *41*, 8075–8098; b) W. Yu, M. D. Porosoff, J. G. Chen, *Chem. Rev.* **2012**, *112*, 5780–5817.
- [3] a) J. Yin, S. Shan, L. Yang, D. Mott, O. Malis, V. Petkov, F. Cai, M. Shan Ng, J. Luo, B. H. Chen, M. Engelhard, C.-J. Zhong, *Chem. Mater.* **2012**, *24*, 4662–4674; b) B. N. Wanjala, J. Luo, R. Loukrakpam, B. Fang, D. Mott, P. N. Njoki, M. Engelhard, H. R. Naslund, J. K. Wu, L. Wang, O. Malis, C. J. Zhong, *Chem. Mater.* **2010**, *22*, 4282–4294; c) D. Wang, H. L. Xin, R. Hovden, H. Wang, Y. Yu, D. A. Muller, F. J. DiSalvo, H. D. Abruña, *Nat. Mater.* **2013**, *12*, 81–87; d) F. Tao, M. E. Grass, Y. Zhang, D. R. Butcher, J. R. Renzas, Z. Liu, J. Y. Chung, B. S. Mun, M. Salmeron, G. A. Somorjai, *Science* **2008**, *322*, 932–934; e) D. I. Enache, *Science* **2006**, *311*, 362–365; f) F. Besenbacher, I. Chorkendorff, B. S. Clausen, B. Hammer, A. M. Molenbroek, J. K. Nørskov, I. Stensgaard, *Science* **1998**, *279*, 1913–1915; g) F. Studt, F. Abild-Pedersen, T. Bligaard, R. Z. Sorensen, C. H. Christensen, J. K. Nørskov, *Science* **2008**, *320*, 1320–1322.
- [4] J. Greeley, I. E. L. Stephens, A. S. Bondarenko, T. P. Johansson, H. A. Hansen, T. F. Jaramillo, Rossmeisl, Chorkendorff, J. K. Nørskov, *Nat. Chem.* **2009**, *1*, 552–556.
- [5] S. Lu, C. Zhang, Y. Liu, *Int. J. Hydrogen Energy* **2011**, *36*, 1939–1948.
- [6] H. Duan, D. Wang, Y. Kou, Y. Li, *Chem. Commun.* **2013**, *49*, 303–305.
- [7] W. Ye, H. Kou, Q. Liu, J. Yan, F. Zhou, C. Wang, *Int. J. Hydrogen Energy* **2012**, *37*, 4088–4097.
- [8] C. Xu, Q. Li, Y. Liu, J. Wang, H. Geng, *Langmuir* **2012**, *28*, 1886–1892.
- [9] H. M. Song, D. H. Anjum, R. Sougrat, M. N. Hedhili, N. M. Khashab, *J. Mater. Chem.* **2012**, *22*, 25003–25010.
- [10] J. Zhang, K. Sasaki, E. Sutter, R. R. Adzic, *Science* **2007**, *315*, 220–222.
- [11] G. Chen, S. Desinan, R. Nechache, R. Rosei, F. Rosei, D. Ma, *Chem. Commun.* **2011**, *47*, 6308–6310.
- [12] G. Chen, S. Desinan, R. Rosei, F. Rosei, D. Ma, *Chem. Eur. J.* **2012**, *18*, 7925–7930.
- [13] C. Solliard, M. Flueli, *Surf. Sci.* **1985**, *156*, 487–494.
- [14] K. W. Park, J. H. Choi, B. K. Kwon, S. A. Lee, Y. E. Sung, H. Y. Ha, S. A. Hong, H. Kim, A. Wieckowski, *J. Phys. Chem. B* **2002**, *106*, 1869–1877.
- [15] a) N. C. Barnard, S. G. R. Brown, F. Devred, J. W. Bakker, B. E. Nieuwenhuys, N. J. Adkins, *J. Catal.* **2011**, *281*, 300–308; b) J. Wang, G. Fan, F. Li, *RSC Adv.* **2012**, *2*, 9976–9985; c) Y. Goto, K. Taniguchi, T. Omata, S. Otsuka-Yao-Matsuo, N. Ohashi, S. Ueda, H. Yoshikawa, Y. Yamashita, H. Oohashi, K. Kobayashi, *Chem. Mater.* **2008**, *20*, 4156–4160; d) S. Sarkar, A. K. Sinha, M. Pradhan, M. Basu, Y. Negishi, T. Pal, *J. Phys. Chem. C* **2011**, *115*, 1659–1673.
- [16] J. H. Jeong, J. W. Lee, D. J. Seo, Y. Seo, W. L. Yoon, D. K. Lee, D. H. Kim, *Appl. Catal. A* **2006**, *302*, 151–156.
- [17] C. Ronning, H. Feldermann, R. Merk, H. Hofsäuss, P. Reinke, J. U. Thiele, *Phys. Rev. B* **1998**, *58*, 2207–2215.
- [18] a) N. Chakroune, G. Viau, S. Ammar, L. Poul, D. Veautier, M. M. Chehimi, C. Mangeney, F. Villain, F. Fiévet, *Langmuir* **2005**, *21*, 6788–6796; b) Y. Yamauchi, T. Ohsuna, K. Kuroda, *Chem. Mater.* **2007**, *19*, 1335–1342; c) K. Lasch, L. Jörissen, J. Garcke, *J. Power Sources* **1999**, *84*, 225–230.
- [19] S. Miao, Z. Liu, B. Han, J. Huang, Z. Sun, J. Zhang, T. Jiang, *Angew. Chem. Int. Ed.* **2006**, *45*, 266–269; *Angew. Chem.* **2006**, *118*, 272–275.
- [20] H. H. Brongersma, M. Draxler, M. de Ridder, P. Bauer, *Surf. Sci. Rep.* **2007**, *62*, 63–109.
- [21] a) M. Zahmakiran, Y. i. Tonbul, S. Özkaz, *J. Am. Chem. Soc.* **2010**, *132*, 6541–6549; b) M. Zahmakiran, S. Özkaz, *Langmuir* **2008**, *24*, 7065–7067; c) G. Süß-Fink, B. Mollwitz, B. Therrien, M. Dadrás, G. Laurenczy, A. Meister, G. Meister, *J. Cluster Sci.* **2007**, *18*, 87–95; d) M. Takasaki, Y. Motoyama, K. Higashi, S. H. Yoon, I. Mochida, H. Nagashima, *Chem. Asian J.* **2007**, *2*, 1524–1533.
- [22] L. Zhu, L. Zheng, K. Du, H. Fu, Y. Li, G. You, B. H. Chen, *RSC Adv.* **2013**, *3*, 713–719.

Received: January 29, 2014

Revised: March 8, 2014

Published online on June 2, 2014